Effect of Membrane Microheterogeneity and Domain Size on Fluorescence Resonance Energy Transfer

Kevin B. Towles, Angela C. Brown, Steven P. Wrenn, and Nily Dan
Department of Chemical and Biological Engineering, Drexel University, Philadelphia, Pennsylvania

ABSTRACT Studies of multicomponent membranes suggest lateral inhomogeneity in the form of membrane domains, but the size of small (nanoscale) domains in situ cannot be determined with current techniques. In this article, we present a model that enables extraction of membrane domain size from time-resolved fluorescence resonance energy transfer (FRET) data. We expand upon a classic approach to the infinite phase separation limit and formulate a model that accounts for the presence of disklike domains of finite dimensions within a two-dimensional infinite planar bilayer. The model was tested against off-lattice Monte Carlo calculations of a model membrane in the liquid-disordered (l_d) and liquid-ordered (l_o) coexistence regime. Simulated domain size was varied from 5 to 50 nm, and two fluorophores, preferentially partitioning into opposite phases, were randomly mixed to obtain the simulated time-resolved FRET data. The Monte Carlo data show clear differences in the efficiency of energy transfer as a function of domain size. The model fit of the data yielded good agreement for the domain size, especially in cases where the domain diameter is $<$20 nm. Thus, data analysis using the proposed model enables measurement of nanoscale membrane domains using time-resolved FRET.

INTRODUCTION

Membrane structures, referred to as lipid rafts, are thought to play a role in cellular processes such as signal transduction, protein stabilization, protein and lipid sorting, and membrane fusion (1). Systematic studies of complex native membranes are difficult (1,2), leading to interest in the study of relevant model systems constructed of binary or ternary mixtures of cholesterol, saturated lipid, and/or unsaturated lipid (2). Techniques used to detect membrane domains, such as fluorescent microscopy (3), differential scanning calorimetry (4), nuclear magnetic resonance (5), fluorescent correlation spectroscopy (6), small-angle neutron scattering (7), and fluorescent resonance energy transfer (FRET) (8) provide evidence for lateral organization on two distinct length scales—microns and nanometers (3,7,9,10). Yet, despite intensive efforts, little is known regarding the presence and properties of nanoscale domains in either cellular (2,9,11) or model (2,3,12) membranes. Thus, there is a critical need for quantitative tools that can resolve lipid organization on nanometer length-scales.

FRET has been used for decades to probe atomic length-scales (13) by measuring the difference between donor fluorophore decays in the presence and absence of an acceptor fluorophore. The sensitivity of FRET to distances that range from 1 to 10 nm in bulk, and slightly extended values in a planar geometry such as a bilayer (9,14), has been exploited to study protein conformational changes (15), protein complexation (16,17), and structural transitions in membranes (18) (for additional applications; see, for example, (19,20)).

Preferential sequestering of one probe, of a donor-acceptor pair, into bilayer structures or domains, should lead to a reduction in energy transfer, whose magnitude reflects the degree of probe partitioning and the domain size. Recent studies have demonstrated this effect in model membranes (9,21,22). However, while analytical expressions exist for populations of homogeneously distributed fluorophores (13,23) and distributions with excluded volume (24), there are currently no analytical models that can be used to correlate the fluorescence decay profile to the size of finite membrane domains.

In this article, we develop a quantitative model to enable the analysis of time-resolved fluorescence decay profiles within lipid bilayers that display two-phase coexistence, with the goal of determining characteristic domain size. The model accounts for the random distribution of donor and acceptor molecules (subject to probe partition coefficients) both inside and outside domains. Using the classic approach developed by Wobler and Hudson (23) and expanding upon previous work (9,23–25) using the so-called infinite phase separation limit, we obtain an analytical approximation for the case of finite domains. Combining our approximation with numerical fits of simulated acceptor distributions, we develop a powerful tool for the analysis of time-resolved FRET data that is theoretically applicable to any donor-acceptor pair.

Evaluation of the model applicability requires testing on data from membranes with well-characterized domains. Since direct, noninvasive techniques for measuring domain size are, as yet, unavailable, we chose to apply our model to data from off-lattice Monte Carlo calculations. These Monte Carlo calculations, which have been widely used to produce FRET data (8,13) and have even been able to reproduce experimental data (see, for example, (26)), are of a static lipid bilayer and should not be confused with Monte Carlo simulations

Submitted June 5, 2006, and accepted for publication March 13, 2007.

Address reprint requests to K. B. Towles, Tel.: 215-895-5938; E-mail: kbt22@drexel.edu.

Editor: Akihiro Kusumi.

0006-3495/07/07/655/13 $2.00

doi: 10.1529/biophysj.106.090274

used to estimate membrane thermodynamic properties (see, for example, (27)). The parameters chosen for the Monte Carlo calculations are representative of model membranes that display coexistence between liquid-disordered (l_d) and liquid-ordered (l_o) domains (see Fig. 1).

The Monte Carlo calculated FRET efficiencies clearly show high sensitivity to domain sizes in the range of 5–50 nm. Applying our analytical model to the data obtained from the Monte Carlo calculation yields values for the domain diameter that are within ~20% of the input value for domains of diameter less than four times the Förster radius of the donor-acceptor pair (which typically ranges between 1 and 10 nm). Thus, analysis of FRET data using our model can provide an accurate method for determining the size of membrane domains of order <40 nm, which could not be probed, in situ, by other techniques.

RESONANCE ENERGY TRANSFER

Fluorescence resonance energy transfer, or resonance energy transfer, describes a process in which a donor fluorophore is excited by incident light and undergoes a nonradiative decay to a nearby acceptor fluorophore (19). The term fluorescence resonance energy transfer can actually be somewhat misleading because, when FRET occurs, the donor does not actually emit a photon; instead, the energy absorbed from the incident photon is transferred via a dipole-dipole interaction to a nearby acceptor. Actually, the theory of energy transfer

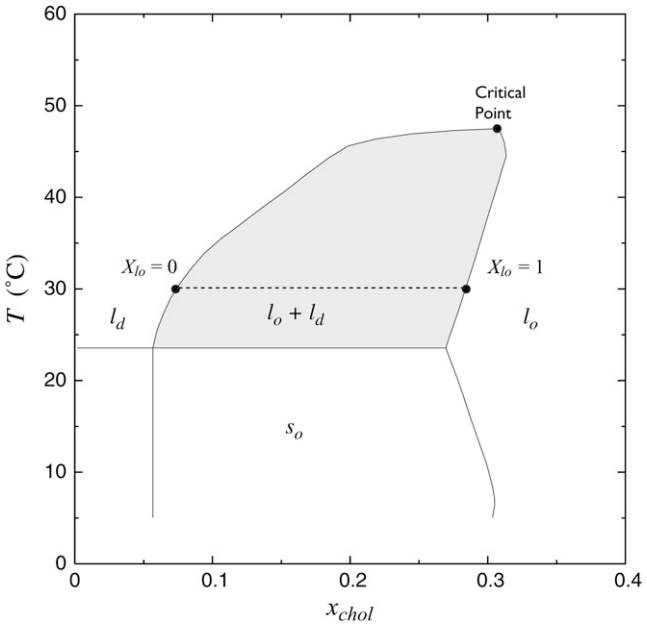

FIGURE 1 Phase diagram for the DMPC/cholesterol system plotted as a function of the overall cholesterol mol fraction, x_{chol} (30). The shaded area is the two-phase, $l_o + l_d$, coexistence region, and the dashed line within this region is the tie-line (30°C) on which all calculations in this study were conducted.

was developed by treating a fluorophore as an oscillating dipole that can interact with other nearby oscillating dipoles with similar resonance frequencies (19) (a classic metaphor is two swinging pendulums connected by a spring). The distance at which this transfer is 50% efficient is called the Förster distance, R_0, and the rate of energy transfer is governed by the dipole-dipole interaction and scales as r^{-6}, where r is the donor-acceptor distance (28). This strong distance-dependence gives FRET its sensitivity to nanometer distances, and the fluorescence decay contains a wealth of structural information regarding the environment of the donor-acceptor pair (19). While characterizing FRET between a single donor-acceptor pair is quite simple, complex expressions are required to describe FRET among populations of fluorophores interacting in restricted geometries.

MODEL

In this section, we present a model for FRET in a phase-separated lipid bilayer system containing finite domains. Two types of FRET probes, one donor and one acceptor, partition in an unequal manner between the bilayer domains, as has been shown experimentally (8,21). Due to its inherent complexity, we present the model in two subsections. The first subsection briefly outlines the tenets of the model and describes the general flow of how one might use it to determine the intensity decay of donors in the presence of a heterogeneous acceptor distribution and ultimately obtain information regarding the size of domains. For those interested in the complete details, the second subsection provides a step-by-step derivation.

OVERVIEW

The major contribution of this study is to provide a method for estimating donor decays in the presence of heterogeneous acceptor distributions. To do so, we essentially take two key steps forward: first, we derive new analytical expressions for donor decay to heterogeneously distributed acceptors, and, second, we approximate heterogeneous acceptor populations for donors inside/outside domains of different sizes.

Analytical expressions exist for estimating the donor decay with an exclusion zone of radius R_e (when R_e is of the same order as R_0) within which acceptors are not found (9,23,24). We modified existing expressions to estimate the contribution of acceptors confined to a shell, or annulus. Assuming the density of acceptors in that shell is constant, we can estimate the contribution to the decay from acceptors within that shell at a given density. Summing up the contributions from shells over all space (from both inter- and intraplanar acceptors), we arrive at an expression for the intensity decay for a donor with a known acceptor density profile.

The first step in estimating acceptor distributions was to obtain an expression for the probability of finding a domain at some distance, r. We make use of a mean-field approximation

to numerically estimate the average probability of finding a domain at some distance r from a random point of origin. While the probability of finding domains at large distances from the origin should converge to the bulk surface coverage of domains, the behavior near the point of origin depends strongly on whether the origin lies inside or outside a domain and its proximity to nearby domains. Therefore, we obtain independent approximations for points (donors) originating inside or outside domains. Numerically obtained profiles are fit with a decaying exponential as a function of the dimensionless distance r/D_d for each surface coverage. The result is an approximation for the mean-field probability of finding a domain as a function of distance, $\langle\sigma(r)\rangle$, for any domain size and surface coverage. Since we can calculate the acceptor density both inside and outside domains from the partition coefficients, estimating the mean-field acceptor distribution is a simple weighting of acceptor densities in each phase by the probability of finding a domain at any particular distance.

Finally, we sum the weighted contributions (as set by the donor partition coefficient) of donors both inside and outside domains to obtain a final expression for the intensity decay as a function of the surface coverage and domain diameter. Once we have an expression for the intensity decay, we can easily estimate the efficiency of energy transfer or fit existing decay profiles to obtain an estimate of the domain diameter.

DERIVATION

The model presented here is applicable assuming the following can all be estimated: the phase boundaries and compositions in each phase (for binary systems, this is relatively simple; however, estimating compositions in ternary systems is more complex), the area per lipid in each phase, the position of the donor/acceptor chromophore relative to the lipid-water interface, and the Förster radius, R_0. The implications of these assumptions and a discussion of error related to them are expanded upon in Discussion and Conclusions.

The FRET-related function for in-plane decay (see Fig. 2) of the donor species in the presence of acceptors with an excluded radius for acceptors, R_e in an infinite, homogeneous planar bilayer where all components are randomly distributed in both leaflets has been previously derived (9,23,24) as

$$\rho_{cis}(t) = \exp\left\{-\pi R_0^2 n\gamma\left[\frac{2}{3}, \left(\frac{R_0}{R_e}\right)^6 (t/\bar{\tau})\right](t/\bar{\tau})^{1/3} + \pi R_e^2 n\left(1 - \exp\left[-\left(\frac{R_0}{R_e}\right)^6 (t/\bar{\tau})\right]\right)\right\}, \quad (1)$$

where R_0 is the Förster radius, n is the surface density of acceptors, $\bar{\tau}$ is the lifetime-weighted quantum yield given as (19)

$$\bar{\tau} = \sum_i \alpha_i \tau_i, \quad (2)$$

and the incomplete Gamma function is defined as

$$\gamma(x, y) = \int_0^y z^{x-1}\exp(-z)\, dz. \quad (3)$$

The donor decay to the opposite leaflet (see Fig. 2) in the presence of acceptors is given by (9,23,24)

$$\rho_{trans}(t) = \exp\left\{-\frac{2c}{\Gamma(2/3)b}\int_0^{w/(w^2+R_e^2)^{1/2}} [1 - \exp(-tb^3\alpha^6)]\alpha^{-3}\, d\alpha\right\}, \quad (4)$$

where $b = (R_0/w)^2/\bar{\tau}^{1/3}$, Γ is the complete Gamma function, w is the interplanar donor-acceptor distance, and

$$c = \Gamma(2/3)n\pi R_0^2\bar{\tau}^{-1/3}. \quad (5)$$

Equations 1 and 4 assume that the Förster radius is invariant; in fact, the value of R_0 may vary among donor and acceptor pairs in the membrane due to its dependence on several factors including the rotational freedom of the fluorophores, the refractive index of the medium, spectral overlap, and the quantum yield of the donors. However, as will be discussed later, variations in the value of R_0, and consequently error in the model itself, can be minimized through thoughtful experimental design.

In the case of a single phase, the donor decay in the presence of acceptors becomes

$$i_{DA}(t) = i_D(t)\rho_{cis}(t)\rho_{trans}(t), \quad (6)$$

where the donor decay in the absence of acceptors is given by a single exponential decay as $i_D(t) = \exp(-t/\tau)$. In the case of no domains, the distance of closest approach, R_e, is defined as the sum of the van der Waals radii of the acceptor-donor pair. Therefore, estimating the decay of a donor in the l_d phase is a straightforward application of Eqs. 1–6. However, if the membrane consists of two coexisting phases (e.g., l_o and l_d), then the donor decay function can be estimated in the presence and absence of acceptors as a weighted average of the contributions of each phase as

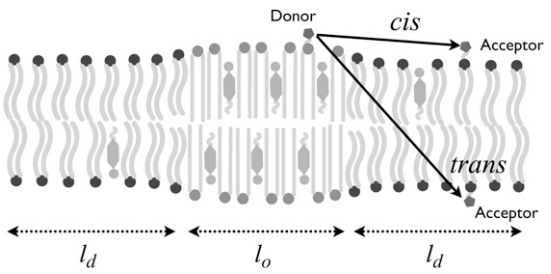

FIGURE 2 Cross-sectional cartoon of a phospholipid and cholesterol lipid bilayer containing liquid-ordered, l_o, lateral heterogeneity. Resonance energy transfer from the donor to an in-plane acceptor is denoted by *cis*, and transfer to an acceptor in the opposite leaflet is denoted *trans*.

$$i_{DA}(t) = \sum_{l} P_l i_{Dl}(t)\rho_{cis,l}(t)\rho_{trans,l}(t), \quad (7)$$

$$i_{D}(t) = \sum_{l} P_l i_{Dl}(t), \quad (8)$$

where P_l is the mole fraction of donors in phase l, $i_{Dl}(t)$ is the decay of the donor in the absence of acceptor in phase l, and both $\rho_{cis,\,l}(t)$ and $\rho_{trans,\,l}(t)$ are calculated as a single phase situation (with appropriate parameters specific to each phase). Eq. 7 is the infinite phase separation approximation, which essentially treats the two donor populations (one in each phase) as independent, isolated populations. For a two-phase, l_o and l_d bilayer, we define two partition coefficients, k_A and k_D for the acceptor and donor, respectively, as

$$k_{A(D)} = \frac{P_{lo}/X_{lo}}{P_{ld}/(1 - X_{lo})}, \quad (9)$$

where P_{lo} and P_{ld} are the fractions of the probe in the l_o and l_d phases, respectively, such that $P_{lo} + P_{ld} = 1$, and X_{lo} is the mole fraction of the membrane that is in the l_o phase. The area fraction of the membrane in the liquid-ordered phase is written as

$$\sigma_\infty = \frac{A_{lo} \times X_{lo}}{A_{lo} \times X_{lo} + A_{ld}(1 - X_{lo})}, \quad (10)$$

where A_{lo} and A_{ld} are the area per lipid of the liquid-ordered and -disordered phases, respectively. The density of acceptors in the bulk, and the relative densities in each phase are

$$n_\infty = \frac{x_A}{A_{lo} \times X_{lo} + A_{ld}(1 - X_{lo})}, \quad (11)$$

$$n_{lo} = \frac{x_A \times k_A}{A_{lo}(1 - X_{lo}(1 - k_A))}, \quad (12)$$

$$n_{ld} = \frac{x_A}{A_{ld}(1 - X_{lo}) + A_{ld} \times X_{lo} \times k_A}, \quad (13)$$

where x_A is the mole fraction of acceptors in the system.

Here we revise this model to account for the formation of monodisperse domains of diameter D_d as one of the two phases. In the case of domain formation, the bilayer contains two separate phases with different probe partitioning that exist simultaneously; consequently, two different populations of acceptors must be considered to determine the decay of a donor in such a domain accurately. A donor existing within a domain has a distance of closest approach for an acceptor in the same phase equivalent to that of the single phase case; however, the distance of closest approach to an acceptor in the phase outside that domain is dependent on the location of the donor relative to the domain. One way of taking these boundary effects into account is to describe the system in terms of ensemble average behavior and look at discrete distances from an average donor within that system.

We modify the approach of Loura et al. (8,9) to calculate the contribution to the donor decay of acceptors populating a shell of thickness δ at any distance $r - \delta/2 \le r \le r + \delta/2$ from the donor. Recall that the contributions of the acceptors in both leaflets are calculated as the product of the two individually. In the same manner, the donor decay in the presence of acceptors confined to that shell can be estimated as

$$i_{DA}(t)_{shell} = i_D(t)\frac{[\rho_{cis}(t)\rho_{trans}(t)]_{R_e=r-\delta/2}}{[\rho_{cis}(t)\rho_{trans}(t)]_{R_e=r+\delta/2}}, \quad (14)$$

where the density, n, is now the density of acceptors within that shell, n_{shell}. The donor decay for an infinite series of such shells becomes

$$i_{DA}(t) = i_D(t)\prod_{i=1}^{\infty}\frac{[\rho_{cis}(t)\rho_{trans}(t)]_{R_e=\delta\cdot i}}{[\rho_{cis}(t)\rho_{trans}(t)]_{R_e=\delta(i+1)}}, \quad (15)$$

where the concentration in each shell is given by n_i. Now that we have an expression for the donor decay that is effectively dependent on the concentration of acceptors as a function of distance from the donor, we need to develop expressions for the distribution of acceptors at any distance, $n_i(r)$ for donors inside or outside domains.

First, we approximate the radial distribution function (RDF), which is related to the probability of finding a domain at some distance, of an average donor for a system containing monodisperse domains of diameter, D_d. Analytical expressions for the average RDF of a donor placed randomly either inside or outside one of these domains are, to the best of our knowledge, not available, and their derivation is certainly nontrivial. Therefore, the RDFs for donors in a planar geometry containing nonoverlapping randomly placed monodisperse domains of diameter, D_d, were obtained numerically (for details of the RDF simulations and subsequent fits, see Supplementary Material). The ensemble-averaged RDF for donors inside and outside domains, $\langle g_{in}(r)\rangle$ and $\langle g_{out}(r)\rangle$, are related to the average surface coverage as

$$\langle\sigma_{in}(r)\rangle = 1 - (1 - \sigma_\infty) \times \langle g_{in}(r)\rangle, \quad (16)$$

$$\langle\sigma_{out}(r)\rangle = \sigma_\infty \times \langle g_{out}(r)\rangle, \quad (17)$$

where the average surface coverage, $\sigma(r)$, corresponds to the probability of finding a domain at some distance r from a donor located either inside or outside a domain. Now that we have expressions for the ensemble-averaged surface coverage as a function of distance from donors either inside or outside domains, we can estimate the acceptor density as function of distance from a donor as

$$\langle n(r)\rangle = n_{lo} \times \langle\sigma(r)\rangle + n_{ld}(1 - \langle\sigma(r)\rangle), \quad (18)$$

which can be applied for donors either inside or outside their domains, as long as the corresponding average surface coverage is used. The above formula is used to estimate the acceptor density within the shell as the acceptor density at the center of that shell. This formula is general for any value of probe partitioning; the acceptor partitioning is accounted for through the definitions of n_{lo} and n_{ld} as in Eqs. 12 and 13, and the donor partitioning sets the relative amounts of donor in each phase (see Eq. 7). Therefore, combination of Eqs. 1–10, and 12–18 provides a closed set of equations for the decay

function of donors in the presence and absence of acceptors in a bilayer containing finite domains for any probe partitioning. The efficiency of energy transfer can then be calculated as

$$E = 1 - \left(\int_0^\infty i_{DA}(t)dt\right) \Big/ \int_0^\infty i_D(t)dt. \qquad (19)$$

MONTE CARLO CALCULATIONS

Off-lattice calculations using a Monte Carlo method are conducted on a system modeled after mixtures of phospholipid and cholesterol, which are proposed to exhibit coexistence between liquid-disordered and liquid-ordered domains (see Fig. 1). The model system contains four membrane components: cholesterol, phospholipid, donor, and acceptor; however, since the donor and acceptor are the only interacting components and each of these represents a relatively small portion of the membrane ($<\sim$1 mol %), we consider both cholesterol and phospholipid as inert species with only volume-packing and mass-balancing properties. Therefore, the calculations consider an effective two-component system comprised of only donor and acceptor probes.

Lattice models have been used to describe lateral distribution of membrane components (8,22); however, the restricted geometry of a lattice system precludes the existence of truly circular domains and makes approximations regarding the size of individual components. Therefore, we apply an off-lattice approach to model a square section of a bilayer assuming planar geometry and periodic boundary conditions (although it seems likely that the planar geometry may not apply to small vesicles, it has been shown that even highly curved bilayers produce nearly identical transfer efficiencies to their planar counterparts (29)). The system is illustrated in Fig. 3, where the inner box represents the actual box size. The box size is calculated for each acceptor density and domain radius pair. In keeping with the periodic boundary conditions, all acceptors within four-times the Förster radius of the donor-acceptor pair (a distance at which 99.98% of all decay occurs) of the box perimeter were kept to ensure proper interactions for donors within the box area. Calculation results were identical for cases where this distance was increased severalfold. The relative number of donors and acceptors in each phase is set by the partition coefficient (Eq. 9). The placement of l_o domains, donors, and acceptors were all completely random subject to only two constraints: nonoverlap of domains and nonoverlap of probes. Domains are assumed symmetric and vertically coupled in the two leaflets of the bilayer. All calculations contain at least 10^3 probes of each type in the bilayer, and time-resolved data are then averaged over tens of runs.

Since the locations of all donors and acceptors are known, calculating the time-resolved decay data is trivial, as detailed in the series of equations below (28). The fluorescence decay

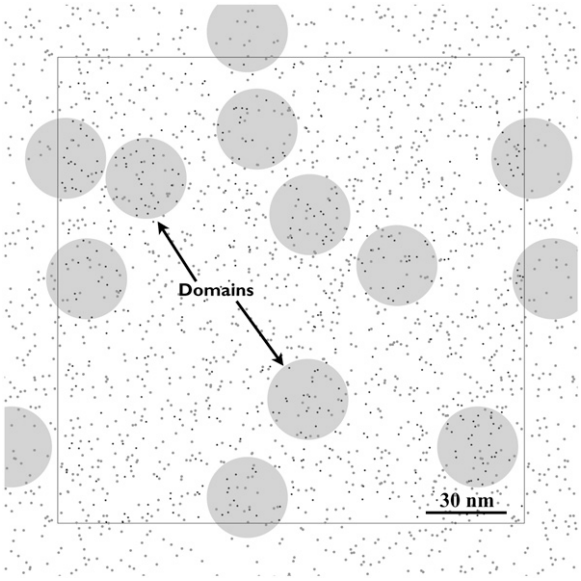

FIGURE 3 This is a top-down view of the simulated bilayer with $X_{lo} = 0.25$, and the actual calculation box is the area within the inner square outline. All acceptors within the cutoff range of the box edge (4 R_0) are retained. Domains appear as the large light-shaded circles ($D_d = 30$ nm), acceptors the small, light-shaded circles, and donors the small, darkest circles. Probes in both leaflets of the bilayer are shown so there may appear to be overlap, but within each leaflet there is none (scale bar = 30 nm).

function for a single donor, j, located in phase i in the presence of multiple acceptors is given as

$$\rho_{ijDA}(t) = \exp\left(\frac{-t}{\tau_i}\right) \prod_{k=1}^{N_A} \exp\left[\left(\frac{-t}{\tau_i}\right)\left(\frac{R_{0i}}{R_{jk}}\right)^6\right], \qquad (20)$$

where τ_i is the fluorescence lifetime of the unquenched donor in phase i, N_A is the total number of acceptors, R_{0i} is the Förster radius for the donor-acceptor pair in phase i, R_{jk} is the pair distance from donor j to acceptor k, and t is time. We assume that the Förster radius is independent of phase and no homo-transfer occurs among donors, implying that no significant spectral shift occurs for probes between phases, the probes are in the dynamic averaging limit, and the Stoke's shift of the donor is large enough to avoid overlap of the donor absorption and emission spectra (additional discussion regarding these assumptions can be found in Discussion and Conclusions). Summing over all of the donors, the average donor decay function in the presence of acceptors becomes

$$i_{DA}(t) = \frac{1}{N_D} \sum_i \sum_{j=1}^{N_{Di}} \rho_{ijDA}(t), \qquad (21)$$

where N_{Di} is the number of donors in phase i and the N_D is the total number of donors defined as $\sum_i N_{Di}$. The average fluorescent decay function for a single donor in the complete absence of acceptors is an average of the decay functions in each phase written as

$$i_D(t) = \frac{1}{N_D}\sum_i N_{Di} \exp\left(\frac{-t}{\tau_i}\right). \quad (22)$$

The efficiency of energy transfer is then calculated by integrating the ratio of the donor decay function in the presence and absence of acceptors over all time as previously defined in Eq. 19.

RESULTS

One of the goals of this article is to develop a quantitative model that relates domain size to FRET in heterogeneous planar bilayers (Eq. 15). However, we first must determine whether FRET in heterogeneous membranes can distinguish between different domain sizes, and, if that is indeed the case, determine the range of domain sizes that FRET can assess within reasonable accuracy. Note that these issues are not specific to the analytical model presented here but are general features of time-resolved FRET experiments. Once it is clear that FRET is sensitive to membrane domain sizes, our analytical model must be tested by application to FRET data where the domain size is known by some other means.

Optimally, testing the model should be carried out on FRET data obtained experimentally from a system with known domain size. However, although several studies find a reduction in FRET efficiency in the two-phase region (8,9), we are not aware of an investigation where the domain size was determined, independently, using some other technique. Indeed, the main driving force for this current work is the difficulty in measuring domains whose size is ~100 nm or less. Thus, to test FRET as a tool for measuring domain size and the validity and limits of our analytical model, we use data obtained from off-lattice Monte Carlo calculations. These calculations, which have been previously applied to such systems with great success (23), produce time-resolved decay data for donors both in the presence and absence of acceptors. To ensure that the parameters used in the calculations are consistent and applicable to model membranes, we chose a typical phase diagram based on DMPC and cholesterol mixtures, as shown in Fig. 1 (30). It should be noted that there is currently a debate whether a two-component membrane can truly exhibit phase coexistence (see, for example, (12)). However, since the goal of our calculations is to provide FRET data that is representative of bilayers composed of two types of domains, this issue is not relevant to our calculations.

The area/lipid of the two phases in our DMPC/cholesterol system were taken from previous estimates to be 0.488 and 0.601 nm^2 (30°C) for the l_o and l_d phases, respectively (8). Due to the lack of experimental data relating the thickness of the bilayer to cholesterol content, the thickness was set at 3.9 nm in both phases (8). All of the calculations are carried out at a fixed system temperature of 30°C; according to the phase diagram for the DMPC/cholesterol system shown in Fig. 1, at 30°C the cholesterol mole fractions are 0.08 and 0.28 in the l_d and l_o phases respectively. The fraction of the system that is in the l_o phase is determined by the inverse lever rule (e.g., an overall cholesterol mole fraction of 0.13 corresponds to a l_o fraction of $X_{lo} = 1/4$). It should be noted that we have assumed throughout this study that the l_o phase is the domain phase; however, it is likely that at large fractions of X_{lo}, an inverted scenario dominates, where the l_d phase becomes the minority, domain phase. Calculations were carried out for domain diameters ranging from 5 to 50 nm for 10 different cholesterol loadings.

We assume typical values for the Förster radius, 5.0 nm for both phases (19,20), and lifetime-weighted quantum yields in the fluid and gel phases, 0.8 and 1.32 ns, respectively (24), for all studies discussed here. The acceptor partition coefficient was held constant at $k_A = 1/4$ to represent a typical membrane probe that prefers the l_d phase (8). The donor partition coefficient was varied from 3/2 to 4 to represent a probe that favors the l_o phase; for comparison, according to the phase diagram in Fig. 1, cholesterol's partition coefficient is 7/2 for the DMPC/cholesterol system at 30°C. A summary of simulated input parameters appears in Table 1.

To examine whether FRET data can distinguish between different domain sizes, we plot in Fig. 4 the efficiency of energy transfer as calculated from the Monte Carlo data, as a function of the mole fraction of the liquid-ordered domain phase (equivalent to the cholesterol content). We see that at any of the examined values of X_{lo}, the efficiency decreases significantly with increasing domain size. For example, at $X_{lo} = 0.291$ ($\sigma_\infty = 0.25$), the efficiency of energy transfer is ~0.45 for the largest possible domain, and 0.65 for 5-nm domains. As may be expected, the sensitivity to domain size is small when the fraction of the minority phase is small (e.g., $X_{lo} < 0.1$), since in such systems most probes are in the continuous majority phase. For a given domain size, we find that the efficiency of energy transfer displays a minimum as a function of the minority phase fraction (Fig. 4 *A*). This behavior may be explained by recalling the definition of the partition coefficient given in Eq. 9: the ratio of probe fraction in each phase, P_{lo}/P_{ld}, scales as $X_{lo}/(1 - X_{lo})$. Therefore, as X_{lo} increases, the balance between the increase in domain density and the increasing probe fraction in the l_o phase (for both probes) can lead to a minimum in the transfer efficiency. Indeed, such minima were observed experimentally for several different probes and acceptor concentrations (9).

It may seem reasonable that the size of membrane domains may be determined from fits to plots of E as a function of X_{lo}, since the depth of the minimum seems to be correlated to the domains size (see, for example, Fig. 4 *A*). While this appears feasible, in many cases the domain size may vary as a

TABLE 1 Range of simulated FRET parameters

D_d	5.0, 7.5, 10, 15, 20, 30, 40, 50
σ_∞	0.05–0.5 (every 0.05)
k_D	1.5, 2, 4
k_A	0.25
x_A	0.005

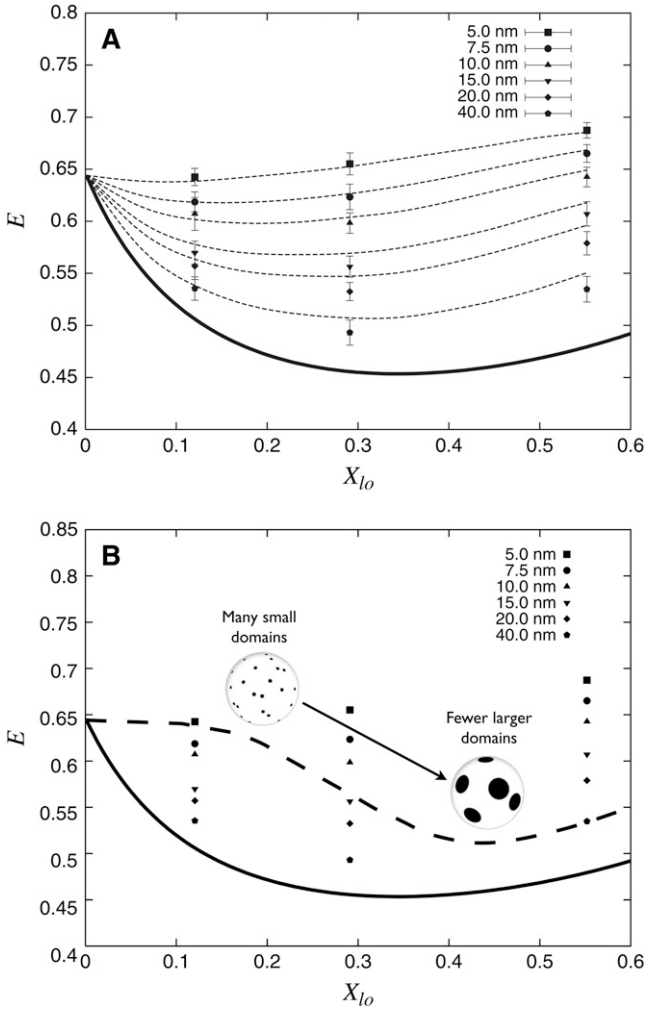

FIGURE 4 (*A*) Simulated efficiency of energy transfer is plotted as a function of liquid-ordered fraction, X_{lo} for domain diameters ranging from 5 to 40 nm. As domain diameter increases, the efficiency of energy transfer decreases at each value of X_{lo}. The thick solid line represents the infinite phase separation limit (see Eq. 7). Data points with error bars represent the simulated efficiency with the associated standard deviation at each point, and the dashed lines are splines of the model predictions for the same set of domain diameters. (*B*) The thick dashed line is a hypothetical trajectory for the same system shown in panel *A*; following the line from left to right illustrates that, as the liquid-ordered fractional coverage increases, the domain size may also be increasing, moving from a vesicle with many small domains to one with fewer, larger domains ($k_D = 4$, $k_A = 0.25$, $\bar{\tau}_{lo} = 1.32$ ns, and $\bar{\tau}_{ld} = 0.8$ ns).

function of membrane composition. For example, consider a trajectory whereby at low liquid-order phase fraction (e.g., $X_{lo} = 0.1$) the domains are of ~5 nm and increase in size with increasing X_{lo} (e.g., 15 nm at $X_{lo} = 0.3$). Since such a trajectory (see Fig. 4 *B*) yields one that is qualitatively similar to the trajectory obtained in the case of constant domains size (Fig. 4 *A*), obtaining domain size from *E*-versus-X_{lo} plots is unreliable unless additional information regarding the system is available. Thus, while the Monte Carlo calculations clearly indicate that FRET data is indeed sensitive to domain sizes in the range of 5–50 nm, a specific model is required to obtain the domain size.

To examine the accuracy and applicability of our analytical model, we first compare the FRET efficiency as predicted by the model to the Monte Carlo calculations (Fig. 4). We see that the efficiency predicted by the analytical model is nearly identical to that of the Monte Carlo calculations for smaller domains (<20 nm) but overpredicts the efficiency in systems with larger domains, thus suggesting that the model will be a useful analysis tool for smaller domains, but may yield less reliable values for larger domains.

By definition, the FRET efficiency is an average over decays of donors in both the presence and absence of donors, and, consequently, contains less information than the time-resolved decay profile. Therefore, estimating the domain diameter by fitting the time-resolved data is a fundamentally better method. In Fig. 5, we plot the time-resolved fluorescence intensity, comparing the analytical model (*lines*) to the Monte Carlo data (*points*). The qualitative agreement between the model and simulated data is apparent for both cases of donors in the presence and absence of acceptors. As in the case of *E*, the quantitative agreement is strong for the smaller domains, and decreases for larger domain diameters. It should be noted that many such tests to verify the applicability of Eq. 15 were conducted, with similar success.

So far we have shown (Figs. 4 and 5) that our analytical model, Eq. 15, yields results that are similar to the Monte Carlo data. However, our goal is to use the analytical model to extract membrane domain size from FRET data. Thus, we need to apply the analytical model to the measured decay profile, extract the model-determined domain size, and compare it to the true value as set in the Monte Carlo calculation.

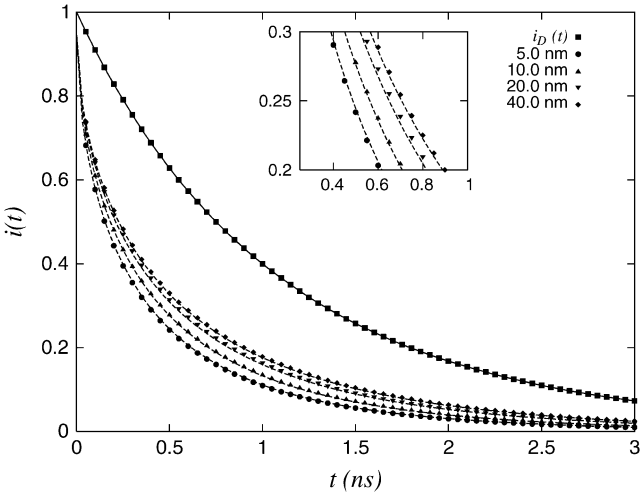

FIGURE 5 Time-resolved fluorescence intensity data is shown for both calculation (*points*) and model (*lines*) for domain diameters from 5 to 40 nm. The solid line is the decay of the donors in the absence of acceptors, $i_D(t)$, and is therefore independent of domain size. The inset is a magnified portion of the same graph, which clearly shows the good fit achieved by the model.

Determining the domain size, using our model, from time-resolved FRET data can be conducted in two ways; in systems where the probe parameters are known, the fit can be conducted with a single variable—the domain size. However, in most cases, parameters related to the probe photophysics (e.g., donor lifetimes) are unknown, thereby requiring a multiparameter fit. Here we focus on the single parameter fit to evaluate the model potential, since, if the single parameter fit is not successful, the model is not usable.

We performed a least-squares fit of the analytical model to the Monte Carlo data using software based on the Levenberg-Marquardt algorithm (31). The values of X_{lo} and x_A are assumed to be known (fixed at their Monte Carlo calculation value), since those are indeed known in most experiments. All model parameters ($k_A, k_D, \bar{\tau}_{lo}, \bar{\tau}_{ld}$) are set at their known Monte Carlo values, except for one—the domain diameter. In all fits the shell thickness, δ, is assumed to be half the average diameter of the two lipid species, a value that corresponds to the largest thickness found to not affect the fitting results.

Table 2 reports the model-predicted domain size for fits to several Monte Carlo input parameters, where $\sigma_\infty = 0.25$, 0.50. We present only a representative fraction of the cases studied that captures the basic qualitative and quantitative features of our results. We find that the single parameter fit provides domain sizes that are within ~20% of the calculation value for domain diameters up to ~15 nm, with an average error of ~10%. This error steadily increases with domain diameter $\geq 4\ R_0$. However, since the model overestimates the domain diameter in every case for the larger domain sizes, model-extracted values may be used as an upper bound in these cases.

There are three possible causes leading to error in model determination of the domain size. First, error in the fitting of the RDF was found to be a significant factor for larger domain sizes. The RDF is cast in terms of the dimensionless distance, r/D_d, and is therefore independent of domain size; however, most of the decay occurs within $2\ R_0$ which, for large domains, corresponds to the steepest portion of the RDF ($r/D_d < 1$). The second possible source of error could be in the calculation of acceptor concentration at finite intervals; this was investigated using a smaller shell thickness and was found to be insignificant (results not shown). Finally, the finite size of the Monte Carlo sample could be another possible source of error. We found that in cases where the number of simulated domains greatly exceeds $\sim 10^3$, the single parameter fits were consistently better than in systems with a smaller number of larger domains. This discrepancy is likely due to the fact that the analytical model is based on an overall average of the system. Practically, while the sample size of the Monte Carlo calculation is limited by computational time, such limitations on sample size are unlikely to arise is any experimental system, thereby eliminating this contribution to the model error.

While the results in Table 2 are given in absolute dimensions, the important underlying scale in the system is the Förster distance, R_0. In our case, $R_0 = 5$ nm, but R_0 is known to vary from 1 to 10 nm for typical probe pairs (19). Thus, we may conclude that the single parameter fit is relatively accurate for domains up to $\sim 4\ R_0$.

It seems reasonable to assume that the size of membrane domains can be determined with greater accuracy when the decay profiles, and similarly the FRET efficiency, are most sensitive to domain size. Although changing probe characteristics such as the Förster distance is difficult, their concentration is easily controlled. In the case of donors that do not undergo homo-transfer, intensity measurements, and consequently the efficiency of transfer, are theoretically independent of donor concentration. However, the concentration of acceptor molecules may affect the efficiency of transfer, and thus measurement accuracy.

In Fig. 6 we examine the effect of acceptor concentration on FRET sensitivity to domain size, defined by the difference, or drop in efficiency between very small domains (5 nm) and the infinite phase separation limit; the larger the difference, the more sensitive the measurement should be to domain size. The three lines represent model prediction at different values of X_{lo}. We find an obvious maximum in ΔE for each X_{lo}, which occurs at $x_A \sim 0.0055$–0.0075. This trend was found for a wide range of k_D, k_A, $\bar{\tau}_{lo}$, and $\bar{\tau}_{ld}$ (results not shown); while the magnitude of ΔE varied for each case, the optimal value of x_A seems independent of all of these

TABLE 2 Best fit domain diameters

$\sigma_\infty = 0.25$				$\sigma_\infty = 0.5$			
	Best fit D_d* (nm)				Best fit D_d* (nm)		
D_d (nm)	$k_D = 1.5$	$k_D = 2$	$k_D = 4$	D_d (nm)	$k_D = 1.5$	$k_D = 2$	$k_D = 4$
5.0	4.64	3.90	4.14	5.0	5.20	5.11	4.53
7.5	7.03	7.77	7.33	7.5	7.40	7.78	7.94
10.0	9.89	10.5	10.5	10.0	10.9	11.3	10.6
15.0	16.5	17.6	15.9	15.0	17.7	20.0	17.7
20.0	24.3	23.4	22.2	20.0	29.1	28.8	26.1
30.0	41.4	35.1	32.7	30.0	41.9	38.8	40.0
40.0	46.3	44.7	48.8	40.0	61.7	55.2	51.9
50.0	67.1	63.8	57.0	50.0	63.3	76.6	87.8.

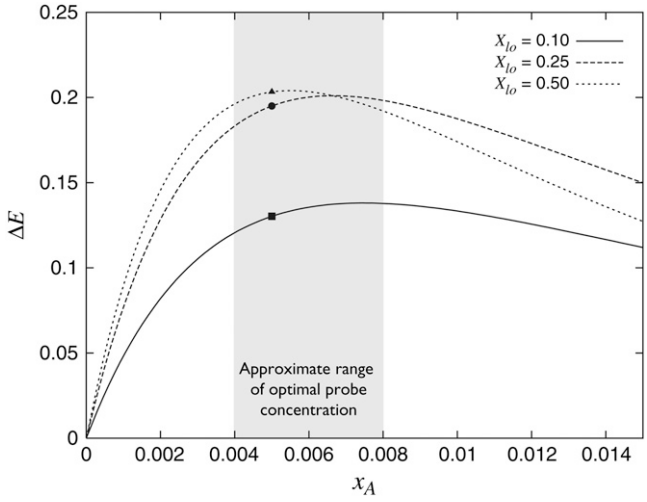

FIGURE 6 The drop in efficiency from small domains (5.0 nm) to the infinite phase separation limit is plotted as a function of the overall mole fraction of acceptors, x_A. The lines represent the model predictions, and the points represent the efficiency drop at the investigated $x_A = 0.005$. An approximate optimal range is shown as the shaded region, where all ΔE are near their maximum values ($k_D = 4$, $k_A = 0.25$, $\bar{\tau}_{lo} = 1.32$ ns, and $\bar{\tau}_{ld} = 0.8$ ns).

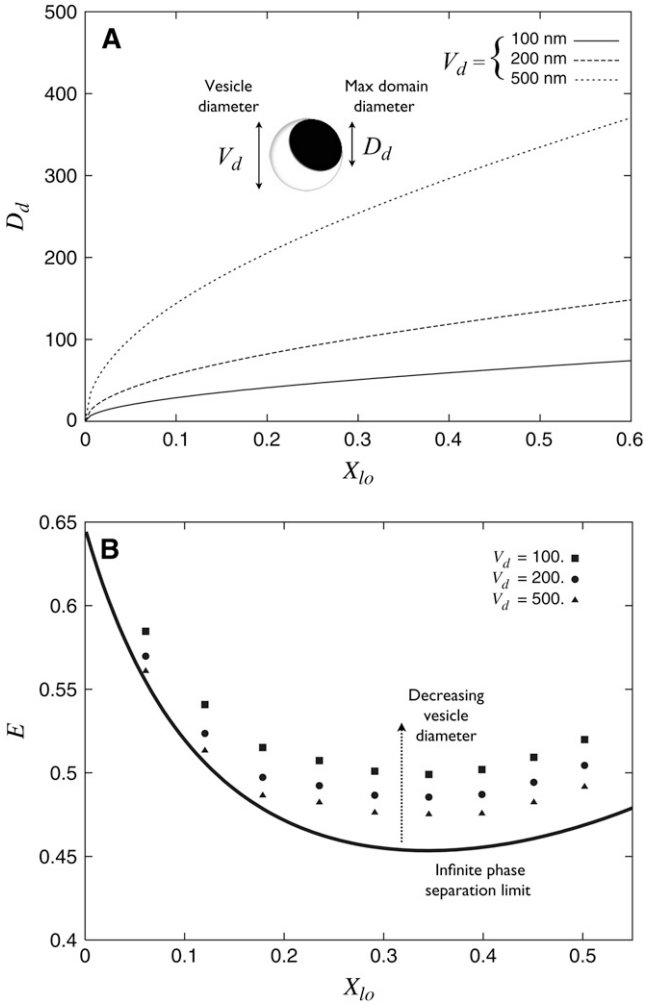

FIGURE 7 Vesicles on the order of 100 nm have different phase separation limits. (*A*) The maximum domain diameter achieved if all of the l_o phase exists as a single domain is plotted as a function of liquid-ordered fraction, X_{lo}, for vesicle diameters of 100, 200, and 500 nm, and (*B*) model estimates of the phase separation limit for the same vesicles are also shown as a function of X_{lo}. These phase separation limits represent the lowest possible energy transfer efficiency for a given vesicle diameter ($k_D = 4$, $k_A = 0.25$, $\bar{\tau}_{lo} = 1.32$ ns, and $\bar{\tau}_{ld} = 0.8$ ns).

parameters. We therefore conclude that there is indeed an optimal range of x_A, which would yield the highest resolution of fit parameters. An approximate optimal range is shown as the shaded region in Fig. 6.

Our model also allows us to reevaluate the limitations of the so-called infinite phase separation limit, which assumes that the relative number of probes at the interface is insignificant compared to those within the domain. The maximum achievable domain size in any given vesicle is limited by the vesicle diameter, V_d, and scales as $V_d \cdot \sigma_\infty^{1/2}$. Fig. 7 *A* plots the maximum domain diameter within vesicles of size $V_d = 100$, 200, or 500 nm; Fig. 7 *B* plots the corresponding model efficiency as a function of X_{lo} for each vesicle size. These results indicate that the infinite phase separation limit for FRET in bilayers is applicable only in vesicles on the order of microns. In vesicles of order <1 μm, the finite size of the maximal single domain must be taken into account.

The single parameter fit is obviously an idealized case. Although a detailed analysis of the multiparameter fit is outside the scope of this article, preliminary results from the multiparameter fit (K.B.T. and N.D., unpublished) suggest that the accuracy of the single parameter fit can be reproduced even in cases where the probe characteristics are not known a priori. An essential feature of the multiparameter fit is global analysis of donor decay data both in the presence and absence of acceptors. Global analysis is the simultaneous analysis of both donor signals, effectively confining three of the common parameters: k_D, $\bar{\tau}_{lo}$, and $\bar{\tau}_{ld}$. Generally, global analysis makes convergence to a single global minimum more likely. To more accurately represent real experimental data, we convoluted the intensity decays with a hypothetical instrument response function and added Poisson noise. Fig. 8 *A* shows one such convolution for the donor in both the absence and presence of acceptors, i_D and i_{DA}, respectively. A practical application of global analysis of FRET signals was done previously by Loura et al. (32); here we will briefly present results of one such fit to prove the practical applicability of our model.

A global fit was performed on our simulated experimental data assuming known partition coefficients, but leaving all other variables as free fit parameters ($\bar{\tau}_{lo}$, $\bar{\tau}_{ld}$, D_d, and the amplitude of each signal). The fit is shown as the solid lines in Fig. 8 *A* and the corresponding weighted residuals, a measure of the deviation at each data point, are shown in Fig. 8, *B* and *C*, for i_D and i_{DA}, respectively. A complete statistical

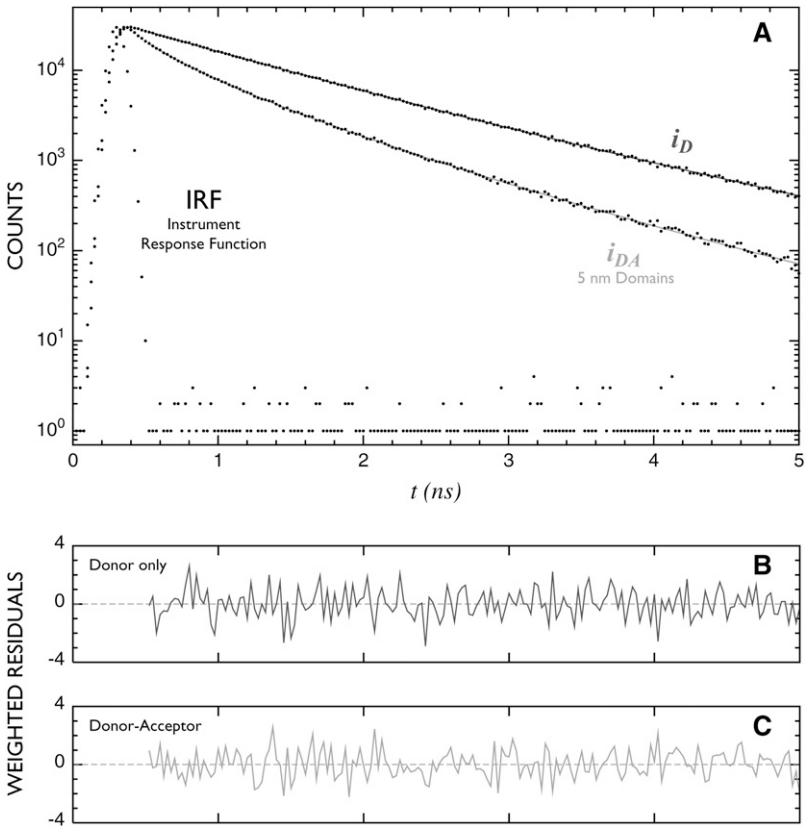

FIGURE 8 Global analysis fit of the intensity decay of donors in the presence and absence of acceptors, i_D and i_{DA}, respectively, after convolution with an instrument response function and the addition of Poisson noise. The data were produced assuming a peak count of 30,000 and channel width of 0.025 ns. (*A*) The fit appears as the solid lines, and the corresponding (*B*) weighted residuals for i_D and (*C*) i_{DA}. The data shown are for a system with $\sigma = 0.1$ for monodisperse domains of size 5.0 nm ($k_D = 4$, $k_A = 0.25$, $\bar{\tau}_{lo} = 1.32$ ns, and $\bar{\tau}_{ld} = 0.8$ ns).

analysis of the results of hundreds of such fits appears elsewhere (33), although the best practical method for obtaining domain size estimates and their appropriate confidence levels for the case of unknown probe partitioning is not, as yet, obvious. However, it seems clear that even poor estimates of the probe partitioning yield similar sensitivity to the domain diameter, and the resulting predictions are distributed about the true domain diameter. Also, to encourage further study we will provide the Mathematica (Wolfram Research, Champaign, IL) code used for fitting such data freely to any interested researchers upon request.

DISCUSSION AND CONCLUSIONS

The ability to accurately determine the presence and dimensions of nanoscale membrane domains is of significant interest for understanding biological membranes. Although several studies indicate the occurrence of nanoscale domains in multicomponent model and cellular membranes (see, for example, (6,7,9,34)), due to experimental limitations little is known regarding the characteristic size of membrane domains or their dependence on system parameters (e.g., temperature or composition).

The sensitivity of FRET to the distance between probes and the tendency of fluorescent probes to partition heterogeneously between different membrane phases suggest that this technique may yield a measure of domain size in situ. Indeed, several studies utilized FRET to detect nanoscale membrane domains (8,9,16,17,22), while Loura and coworkers (8) used FRET to estimate domain dimensions based on the infinite phase separation approximation. Unfortunately, due to the limitations of this approximation their analysis cannot yield a robust quantitative measure of domain size.

The goal of this article is twofold: to establish the sensitivity of time-resolved FRET to the presence and size of membrane domains, and to develop a quantitative model that can be used to extract domain size from such data for bilayers containing multiple acceptor populations.

Using off-lattice Monte Carlo calculations of heterogeneous membranes containing monodisperse, disklike domains we establish that FRET is sensitive to the presence of nanoscale domains with characteristic dimensions ranging from 5 to 50 nm; the efficiency of energy transfer decreases (a consequence of probe partitioning) with domain size at any given liquid-ordered mole fraction, as shown in Fig. 4 *A*. Although FRET is most sensitive when the domains are relatively small, significant differences in the efficiency of energy transfer are found in larger domains (for example, the difference in efficiency at $X_{lo} = 0.291$ and $\sigma = 0.25$ for domains of 50 and 500 nm is 3%). This is quite surprising, since such large domains correspond to diameters of $\geq 10\,R_0$, where the effect of the domain size may be expected to be negligible. The sensitivity of FRET to such large domains must therefore be taken into account in smaller vesicles, where such dimensions

may correspond to the maximal size of a (single) domain, namely, infinite phase separation.

The use of FRET to measure membrane domain size requires a model that accounts for heterogeneous acceptor populations in membranes. Here we develop a theoretical model that quantitatively determines the size of membrane domains from FRET data, based on the one developed by Davenport et al. (25). We find that the model enables determination of the size of domains with diameter of $<4\ R_0$ with a high degree of accuracy ($\sim<20\%$ error). In the case of larger domains, the model-extracted values consistently overestimate domains diameters ($\sim<50\%$ error), thereby providing an upper bound for the domain size. Although the work presented here focused on determining the domain size by assuming that other parameters (i.e., partition coefficients, donor decay time) are known, preliminary results suggest that the domain size may be determined with similar accuracy also in cases where the multiparameter fit is utilized.

Although several simplifying assumptions were made in this work, we expect their effect on the model applicability to be minor. Although noncircular domains are known to form at high temperatures near the critical point (10), our assumption of disklike domains should hold at biologically relevant temperatures where the line tension between the membrane phases is significant. Moreover, in highly asymmetric domains such as two-dimensional ribbons, the transfer efficiency would be dominated by the smaller dimension (width), for which our analysis can be easily modified. Neglecting bilayer curvature is reasonable, since FRET has been shown to be insensitive to membrane curvature even in highly curved bilayers (29). Polydispersity may affect the accuracy of our results, as in any measurement; however, our preliminary data indicate that, at least in moderately polydisperse systems, FRET could yield a reasonable measure of domain size.

The nature of the FRET measurement raises other questions regarding the nature of the probed domains. The typical decay time for FRET probes (nanoseconds (19)) is rapid when compared to the diffusion rate of lipids in the bilayer (order 10^{-8} cm^2/s (35)). Thus, FRET captures a snapshot of membrane organization. It may be argued that 5 nm scale domains observed over such short timescales are due to temporary compositional fluctuations rather than to thermodynamic phase separation. However, distinguishing between these should be simple, since, unlike phase-separated domains, compositional fluctuations are random in size and composition. Also, it is not clear whether the lever rule applies to such small domains, a question that relates to the (as yet unknown) mechanism of domain formation: If domains form through a classical (albeit two-dimensional) nucleation and growth mechanism, the composition of the domain should remain constant with time, fixed at the optimal thermodynamic value even when the domain is the size of the critical cluster ($\sim$5 nm or less) (36). If the domains form through spinodal decomposition, the composition of both domains and the surrounding media will continuously change with time until reaching the thermodynamic value, regardless of the domain size (see, for example, (37,38)). It should be noted that, since the FRET signal is an ensemble measurement obtained from a volume containing numerous vesicles, small local fluctuations in composition would not significantly affect the measurement results. Consequently, conservation of mass will ensure that, on average, the lever rule will apply.

Both the Monte Carlo calculations and the model analysis show that FRET experiments must be planned carefully to enable quantitative measurement of domain size; this topic has also been discussed in a recent review by Loura et al. (14). A number of assumptions, outlined in the model section, necessitate estimates of important membrane parameters. One governing parameter that should be discussed is the estimate of the Förster radius as any error will inevitably effect the scaling of the domain diameter prediction. Typically, the value of R_0 is calculated from

$$R_0 = 0.211\,[\kappa^2\, n^{-4}\, Q_D\, J(\lambda)]^{1/6}\,(\text{in Å}), \tag{23}$$

where κ^2 is the orientation factor, n is the refractive index of the medium, Q_D is the donor quantum yield, and $J(\lambda)$ is the overlap integral in units of M^{-1} cm^{-1} nm^4 with the wavelength, λ, in nm (19). The value of κ^2 ranges from 0 to 4 depending on the orientation of donor and acceptor, and it is typically assumed to be 2/3, the value corresponding to dynamic random averaging (19). Estimating κ^2 is notoriously difficult; however, under typical conditions, error in the estimation of κ^2 leads to $<10\%$ error in R_0 for many FRET pairs (for an excellent discussion of the orientation factor, see Lakowicz (19)). The possibility that R_0 is different for each phase could also introduce error. Previous calculations (8) suggest that the change in the overlap integral alone results in differences of only a few Ångstroms; however, changes in the rotational freedom could potentially cause more significant deviations. It is difficult to definitively state how rotational changes in one phase would affect transfer to probes in the opposite phase; however, considering that changes in κ^2 can result in a maximum of 35% error in R_0 when assuming dynamic random averaging (19), it is expected that only severe changes in the rotational freedom would lead to large error in the estimated R_0, and even then, only the probes in or near domains would be affected. Therefore, in the limit of low surface coverage, such deviations should be relatively small. On the other hand, large deviations in rotational freedom may invalidate the model in the limit of high surface coverage. In fact, any error in the estimation of R_0 may dominate the analysis of domain sizes; while we have not explicitly examined this effect here, there is most certainly a nonlinear dependence of error in the estimation of R_0 on model error. Preliminary results indicate that estimations of R_0 with as little as 5% error yield absolute size estimations with error approaching 100%; however, these results also indicate that the sensitivity to changes in size is comparable to cases where R_0 is known exactly. Thus, important information regarding the evolution of domain size

as a function of domain coverage remains intact. Errors in the estimation of R_0 of >10% may completely invalidate the model; therefore, great care should be taken when obtaining experimental estimates of R_0.

Researchers interested in absolute determinations of domain size should be aware of such issues related to the estimation of the Förster distance. Appropriate choice of fluorophore-labeled probes should minimize the influence of many of these factors. Choosing probes with head-labeled lipids linked with one single or double bond would likely minimize many issues relating to Förster distance estimation (avoid probes with multiple linkage sites between fluorophore and lipid). For example, probes that are head-labeled with one single bond linkage will inherently be more free to rotate than those buried in the lipid bilayer, and they will also likely exhibit larger Stoke's shifts, thereby reducing the influence of homo-transfer. Researchers should always investigate the steady-state absorption and emission spectra of the chosen probes to verify the impact of homo-transfer. Another way to minimize homo-transfer, apart from wise choice of donor probes, is to use acceptor concentrations that are a few fold larger than that of the donor (e.g., a donor concentration of 0.1 mol % and acceptor concentration of 0.5 mol % (8,14)). Even in cases where small amounts of homo-transfer are unavoidable, the effect could be taken into account through the model by including a second acceptor population with R_0 equal to that calculated from the donor emission/absorption spectra. Also, it seems that donors and acceptors with fundamental anisotropies below 0.4, due to overlapping electronic transitions, further constrain the error in the estimation of Förster distances (19,39). Even so, methods for estimating the maximum and minimum κ^2 exist and may be used to better understand the implications for specific systems (19,40,41). Caution must also be taken in choosing appropriate FRET pairs; recent experimental evidence indicates that lipid analogs can exhibit inverse partitioning preference to that of the lipid they mimic (42). Consequently, probe partitioning should be estimated before detailed analysis is carried out. Moreover, the random distribution/aggregation behaviors of the chosen FRET pair should be investigated, although it seems that such effects can be minimized by keeping acceptor and donor concentrations sufficiently below ~1.0% (14). This observation is concurrent with recent discussions of impurities by Veatch et al. (3), which indicate addition of even small amounts (1–3 mol %) of impurities (in the form of proteins, peptides, fluorophores, etc.) can drastically alter membrane properties.

Another important issue is the need, when applying our model, for a priori knowledge of the phase diagram and tie lines. This requirement becomes more complicated as the number of membrane components is increased, although a recent study by Veatch et al. (12) demonstrated the use of nuclear magnetic resonance to estimate both tie-lines and phase compositions in a highly quantitative manner. The area per lipid in each phase is also important for estimating the surface coverage of domains and hence the acceptor distribution.

In conclusion, we show that resonance energy transfer may theoretically be used to accurately determine the size of extremely small membrane domains, of ~1–4 R_0 (typically <40 nm), an observation that has been postulated for some time (23,43), but has never been quantitatively exploited as done here. Larger domains (up to ~10 R_0) may also be investigated using this technique, although with a somewhat reduced degree of accuracy. While our model is developed for membrane domains, it may also be applied to any type of membrane heterogeneity—for example, the distribution of membrane components near embedded proteins.

SUPPLEMENTARY MATERIAL

To view all of the supplemental files associated with this article, visit www.biophysj.org.

This work was supported by the National Science Foundation grant No. ECS 0304453. S.P.W. was supported by the National Institutes of Health grant No. NIGMS R01GM071355, and A.C.B. was supported by the National Science Foundation grant No. CTS 0346638.

REFERENCES

1. Brown, D. A., and E. London. 1998. Functions of lipid rafts in biological membranes. *Annu. Rev. Cell Dev. Biol.* 14:111–136.
2. Simons, K., and W. L. C. Vaz. 2004. Model systems, lipid rafts, and cell membranes. *Annu. Rev. Biophys. Biomol. Struct.* 33:269–295.
3. Veatch, S., and S. Keller. 2005. Seeing spots: complex phase behavior in simple membranes. *Biochim. Biophys. Acta.* 1746:172–185.
4. McMullen, T., and R. McElhaney. 1995. New aspects of the interaction of cholesterol with dipalmitoylphosphatidylcholine bilayers as revealed by high-sensitivity differential scanning calorimetry. *Biochim. Biophys. Acta.* 1234:90–98.
5. Huang, T., C. Lee, A. D. Gupta, R. Blume, and A. Griffin. 1993. A ^{13}C and ^{2}H nuclear magnetic resonance study of phosphatidylcholine/cholesterol interactions: characterization of liquid-gel phases. *Biochemistry.* 32:13277–13287.
6. Korlach, J., T. Baumgart, W. W. Webb, and G. W. Feigenson. 2005. Detection of motional heterogeneities in lipid bilayer membranes by dual probe fluorescence correlation spectroscopy. *Biochim. Biophys. Acta.* 1668:158–163.
7. Pencer, J., T. Mills, V. Anghel, S. Krueger, R. Epand, and J. Katsaras. 2005. Detection of submicron-sized raft-like domains in membranes by small-angle neutron scattering. *Eur. Phys. J. E.* 18:447–458.
8. Loura, L. M. S., A. Fedorov, and M. Prieto. 2001. Fluid-fluid membrane microheterogeneity: a fluorescence resonance energy transfer study. *Biophys. J.* 80:776–788.
9. de Almeida, R. F. M., L. M. S. Loura, A. Fedorov, and M. Prieto. 2005. Lipid rafts have different sizes depending on membrane composition: a time-resolved fluorescence resonance energy transfer study. *J. Mol. Biol.* 346:1109–1120.
10. Baumgart, T., S. T. Hess, and W. W. Webb. 2003. Imaging coexisting fluid domains in biomembrane models coupling curvature and line tension. *Nature.* 425:821–824.
11. Brown, D. A., and E. London. 1997. Structure of detergent-resistant membrane domains: does phase separation occur in biological membranes? *Biochem. Biophys. Res. Commun.* 240:1–7.
12. Veatch, S., K. Gawrisch, and S. Keller. 2006. Closed-loop miscibility gap and quantitative tie-lines in ternary membranes containing diphytanoyl PC. *Biophys. J.* 90:4428–4436.

13. Stryer, L. 1978. Fluorescence energy transfer as a spectroscopic ruler. *Annu. Rev. Biochem.* 47:819–846.

14. Loura, L. M. S., R. F. M. de Almeida, and M. Prieto. 2001. Detection and characterization of membrane microheterogeneity by resonance energy transfer. *J. Fluoresc.* 11:197–209.

15. Heyduk, T. 2002. Measuring protein conformational changes by FRET/LRET. *Curr. Opin. Biotechnol.* 13:292–296.

16. Sharma, P., R. Varma, R. Sarasij, I. K. Gousset, G. Krishnamoorthy, M. Rao, and S. Mayor. 2004. Nanoscale organization of multiple GPI-anchored proteins in living cell membranes. *Cell.* 116:577–589.

17. Varma, R., and S. Mayor. 1998. GPI-anchored proteins are organized in submicron domains at the cell surface. *Nature.* 394:798–801.

18. Snapp, E., G. Reinhart, B. Bogert, J. Lippincott-Schwartz, and S. Ramanujan. 2004. The organization of engaged and quiescent translocons in the endoplasmic reticulum of mammalian cells. *J. Cell Biol.* 164:997–1007.

19. Lakowicz, J. 1999. Principles of Fluorescence Spectroscopy, 2nd Ed. Kluwer Academic/Plenum, New York.

20. Van der Meer, B., G. Coker III, and S.-Y. Chen. 1994. Resonance Energy Transfer: Theory and Data. VCH Publishers, New York.

21. Silvius, R. 2003. Fluorescence energy transfer reveals microdomain formation at physiological temperatures in lipid mixtures modeling the outer leaflet of the plasma membrane. *Biophys. J.* 85:1034–1045.

22. Troup, G. M., T. N. Tulenko, S. P. Lee, and S. P. Wrenn. 2004. Estimating the size of laterally phase separated cholesterol domains in model membranes with Förster resonance energy transfer: a simulation study. *Colloids Surf. B Biointerfaces.* 33:57–65.

23. Wobler, P., and B. Hudson. 1978. An analytical solution to the Förster energy transfer problem in two dimensions. *Biophys. J.* 28:197–210.

24. Davenport, L. 1997. Fluorescence probes for studying membrane heterogeneity. *Methods Enzymol.* 278:487–512.

25. Davenport, L., R. H. Dale, and R. B. Bisby. 1985. Transverse location of the fluorescent probe 1,6-diphenyl-1,3,5-hexatriene in model lipid bilayer membrane systems by resonance energy transfer. *Biochemistry.* 24:4097–4108.

26. Corry, B., D. Jayatilaka, and P. Rigby. 2004. A flexible approach to the calculation of resonance energy transfer efficiency between multiple donors and acceptors in complex geometries. *Biophys. J.* 89:3822–3836.

27. Elliott, R., K. Katsov, M. Schick, and I. Szleifer. 2005. Phase separation of saturated and mono-unsaturated lipids as determined from a microscopic model. *J. Chem. Phys.* 122:044904-1–044904-11.

28. Förster, T. 1949. Experimental and theoretical investigation of the intermolecular transitions of electron excitation energy. *Zeitschrift für Naturforschung A.* 4:321–327.

29. Fung, B., and L. Stryer. 1978. Surface density determination in membranes by fluorescent energy transfer. *Biochemistry.* 17:5241–5248.

30. Almeida, P. F. F., W. L. C. Vaz, and T. E. Thompson. 1992. Lateral diffusion in the liquid-phases of dimyristoylphosphatidylcholine cholesterol lipid bilayers—a free-volume analysis. *Biochemistry.* 31:6739–6747.

31. Gill, P. R., W. Murray, and M. H. Wright. 1981. Practical optimization. *In* The Levenberg-Marquardt Method. Academic Press, London.

32. Loura, L. M. S., A. Fedorov, and M. Prieto. 1996. Resonance energy transfer in a model system of membranes: application to gel and liquid crystalline phases. *Biophys. J.* 71:1823–1836.

33. Towles, K. B., and N. Dan. 2007. Determination of membrane domain size by fluorescence resonance energy transfer: effects of domain polydispersity and packing. *Langmuir.* 23:4737–4739.

34. Pralle, A., P. Keller, E. L. Florin, K. Simons, and J. K. H. Horber. 2000. Sphingolipid-cholesterol rafts diffuse as small entities in the plasma membrane of mammalian cells. *J. Cell Biol.* 148:997–4739.

35. Gennis, R. B. 1989. Biomembranes: Molecular Structure and Function, 1st Ed. Springer-Verlag, New York.

36. Edelstein, A., and R. Cammarata. 1998. Nanomaterials: Synthesis Properties and Applications, 1st Ed. Series in Micro and Nanoscience Technology, Institute of Physics Publishing, Bristol, PA.

37. Haas, C., and J. Torkelson. 1997. Two-dimensional coarsening and phase separation in thin polymer solution films. *Phys. Rev. E.* 55:3191–3201.

38. Marcus, A., D. Hussey, N. Diachun, and M. Fayer. 1995. Nanodomain formation in a liquid polymer blend—the initial stages of phase-separation. *J. Chem. Phys.* 103:8189–8200.

39. Haas, E., E. Katchalski-Katir, and I. Steinberg. 1978. Effect of the orientation of donor and acceptor on the probability of energy transfer involving electronic transitions of mixed polarizations. *Biochemistry.* 17:5064–5070.

40. Corry, B., D. Jayatilaka, B. Martinac, and P. Rigby. 2006. Determination of the orientational distribution and orientation factor for transfer between membrane-bound fluorophores using a confocal microscope. *Biophys. J.* 91:1032–1045.

41. Dale, R., J. Eisinger, and W. Blumberg. 1979. The orientational freedom of molecular probes: the orientation factor in intramolecular energy transfer. *Biophys. J.* 26:161–194.

42. Loura, L. M. S., A. Fedorov, and M. Prieto. 2001. Exclusion of a cholesterol analog from the cholesterol-rich phase in model membranes. *Biochim. Biophys. Acta Biomembr.* 1511:236–243.

43. Dewey, T., and G. Hammes. 1980. Calculation of fluorescence resonance energy transfer on surfaces. *Biophys. J.* 32:1023–1036.